ORIGINAL PAPER

New oxygen evolution anodes for metal electrowinning: MnO$_2$ composite electrodes

Sönke Schmachtel · Martina Toiminen ·
Kyösti Kontturi · Olof Forsén · Michael H. Barker

Abstract Several modifications of manganese dioxide (MnO$_2$) were investigated for use in composite electrode materials for oxygen evolution, the target application being anodes for the industrial electrowinning of metals. It is demonstrated that the performance of this material depends strongly on the modifications of MnO$_2$. All modifications investigated were found to be more active than the usual anode of lead alloyed with silver (PbAg) used in zinc electrowinning. A composite sample containing chemical manganese dioxide (CMD) was found to give an oxygen evolution overpotential 0.25 V lower than the standard PbAg anode material. In the second part of the article, we investigate the effect of varying several parameters of the composite electrode assembly, including the size of the catalyst particles and percentage of the catalyst material used. A model is proposed where the performance of the material is proportional to the total length of the boundaries between the lead matrix material and the MnO$_2$ catalyst particles. Physicochemical processes contributing to the observed data are discussed.

1 Introduction

Oxygen evolution from the oxidation of water (1) is the most common anode or counter reaction in the electrowinning (EW) of metals from acidic sulfate based electrolytes [1]. The oxygen evolution reaction also produces acid [2].

$$H_2O_{(l)} \rightarrow 0.5O_{2(g)} + 2H^+_{(aq)} + 2e^-$$
$$E^o = 1.23 \text{ V vs. SHE} \tag{1}$$
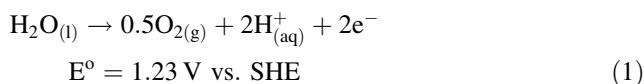
Zinc and copper are the most commonly electrowon metals, whilst nickel, cobalt, chromium, and manganese can also be produced by EW [2]. Zn EW consumes a lot of electrical energy due to the high oxygen evolution overpotential (η_{O_2}), which makes up approximately 0.8 V or 20–25% of the total cell voltage. With the rising cost of energy and environmental concern over the emission of greenhouse gasses, the oxygen evolution overpotential represents a potential area for industry to save energy; even a modest decrease in the η_{O_2} in Zn EW would be of benefit.

Today, the most commonly used EW anodes are still lead based [3–8], for Zn EW lead is typically alloyed with 0.5–1.0 wt% silver. For Cu EW, lead has been alloyed with tin and antimony, and PbCaSn alloys are becoming more common. In general, those alloys used in Cu EW are also suitable for Co and Ni EW. Under electrolysis, the lead anode surface will become oxidised, and the polarization behaviour of the anode material will depend on several variables including the alloy type, the electrolyte composition and the composition of the oxides formed on the anode surface [9].

S. Schmachtel (✉) · M. Toiminen · K. Kontturi (✉)
Laboratory of Physical Chemistry and Electrochemistry,
Helsinki University of Technology, Kemistintie 1,
P.O. Box 6100, 02015 Espoo, Finland
e-mail: sonke.schmachtel@tkk.fi

K. Kontturi
e-mail: kontturi@cc.hut.fi

S. Schmachtel · O. Forsén
Laboratory of Corrosion and Materials Chemistry, Helsinki
University of Technology, Vuorimiehentie 2, P.O. Box 6200,
02015 Espoo, Finland

M. H. Barker
Outotec Research Centre, Kuparitie 10, P.O. Box 69,
28101 Pori, Finland

In a typical Zn EW tankhouse, there is usually manganese present in the electrolyte. The manganese ions are oxidised to MnO_2 at the anode, which collects on the anode surface and often also in the base of the electrolytic cell.

Control of manganese in EW operations is an interesting topic in itself [10, 11] because it is on the one hand intended to decrease the lead anode corrosion, but on the other hand, it requires periodic removal from the cell and from the anodes [12]. Shortening the cleaning intervals means less downtime and increased production.

In the case where manganese is not present in the electrolyte, manganese sulphate can be added to limit anode corrosion [13]. With longer operation times, however, the formation of MnO_2 may increase the corrosion of the lead anode [14]. Decreasing η_{O_2} has also been shown to decrease the total amount of MnO_2 deposited in the Zn EW cell [15].

The literature shows many publications on the modification of lead anodes to improve corrosion resistance [16–18], to enhance the mechanical properties [19] and to save electrical energy [20–22]. There is also interest in improving lead anode performance by pre-treatment [23, 24] or by alloying [25]. Cobalt has been used as an alloying element in anodes used for copper electrowinning [26–29]. Activity and corrosion rates of PbSn(1.4%)Ca (0.12%), PbAg(1%)In(5%), PbRh(0.6%) and PbSnCa with a rhodium coating have been compared with a standard PbAg(0.65%) anode [30]. The use of a lead cobalt alloy for Zn EW, was also reported, the motivation being to identify a cheaper replacement for silver in the commonly used PbAg anode [31].

Another type of anode is the Dimensionally Stable Anode (DSA^{TM}) also known as the Coated Titanium Anode (CTA) [32], which has its origins in the chlor-alkali industry [33–42]. These are usually based on a titanium metal mesh or plate substrate, coated with mixed metal oxides (MMO) of platinum, tantalum, iridium or ruthenium [40, 43].

DSA technology has been adopted in the electroplating industry [44], and for the treatment of wastewaters [45], but is not widely used in EW tankhouses. This is due to not only the traditionally conservative metals industry, but also the high capital investment costs required to purchase the thousands of anodes required for a typical plant, often over 10,000 pieces. The high price of the titanium substrate, the complicated precious metal catalyst coating procedure and the fact that EW applications require high electrode areas, yet employ low current densities, all make it challenging for DSAs to be economically competitive for large-scale EW applications [32].

The surface of DSA coatings are typically described as resembling a 'cracked mud' structure. Under anodic polarization conditions, exposure of the titanium substrate through the cracks allows the growth of an insulating TiO_2 film beneath the active coating, causing loss of the coating and increase in the electrode overvoltage with time [46].

For oxygen evolving anodes, the preferred electrocatalytic coating is IrO_2/Ta_2O_5 [47]. The use of DSAs in EW tend to be in niche applications such as the HPA [48] the RenoCell [45, 49] and EMEW cell types [49, 50].

Another example was reported using a continuous stripping technique operating with an aluminium alloy belt cathode, which employed DSA anodes running at current densities of over 5 kA m^{-2} in purified zinc electrolytes [51].

The Xstrata nickel refinery in Kristiansand, Norway, also uses DSAs in chloride-based EW processes [52, 53]. In Zn EW, however, DSAs have been shown to behave poorly, as the manganese in the tankhouse electrolyte solution causes MnO_2 growth, which blocks the active sites on the coating [54].

The main approach to improving oxygen evolution catalysts has involved varying the precious metal on the surface of a DSA-type electrode [55–57].

In the early 1980s, Beer attempted to decrease the oxygen evolution overpotential and improve the anode performance by incorporating DSA style electrocatalysts on a traditional lead anode base [58, 59]. Another technology uses sponge type titanium electrodes that are filled with lead and sintered [60–62].

The Merrlin composite electrode was also reported, where heat and pressure were used to bind a mixture of lead and manganese oxides onto a lead base. This was claimed to decrease anode scaling and cell sludge in Zn EW, and to reduce the overpotential and corrosion of the electrode [63–65]. It was reported to perform well in industrial large scale (tankhouse) tests, but has not yet been widely adopted in the metals production industry.

There have been many other approaches to modifying the surface of traditional EW anodes, including the DSA mesh on lead approach [66, 67] and protecting the lead anode's surface with conducting polymers [68].

The hydrogen gas diffusion electrode, which eliminates the oxygen evolution reaction at the anode surface, has been investigated for use as EW anodes but with little uptake in industry [69–71].

There have also been reports of modification of the hydrophobicity of oxygen evolving electrodes using PTFE in alkali media [72] and acid media [73].

There are a number of examples of composite materials used for oxygen evolving anodes, such as Co_3O_4 particles [74], mechanically treated SnO_2 [75], $Ir_{0.15}Sn_{0.85}O_2$, [76] and a DSA analogue using MnO_2 on a conductive polymeric substrate of polypropylene, rubber, graphite fibre and carbon black [77].

Due to recent technological advances in spray coating technology [78, 79], Outotec Research has patented a cold

spraying technique for spray coating a catalytically active powder onto a lead anode substrate [80]. The soft mechanical properties of lead alloys used in EW makes it easy to form mechanically robust cold sprayed coatings.

In the present study, we focus on the use of MnO_2 modified lead as an anode material for Zn EW. Use of such MnO_2 coated anodes may have a niche application in solvent extraction (SX)-based electrowinning of zinc, where typically there will be little manganese in the electrolyte [81, 82].

The aim of the present study is to identify suitable, cost effective catalysts, which can be cold spray coated onto a lead anode substrate to produce an analogue of the DSA. Earlier attempts to form in situ coatings on lead anodes gave lower η_{O_2} on short timescales, but the coatings had low durability and were lost to the electrolyte after approximately 1 h of electrolysis, because they were poorly attached to the surface or insufficiently corrosion resistant to the typical strong acid electrolytes used in EW [83].

When cold spray coating onto lead anodes, the coatings on the electrode surface produced electrodes that resemble composite electrodes, because lead, as a soft matrix material, is easily deformed and penetrated by the catalyst particles, leaving a composite coating on top of the standard lead based anode.

This investigation was carried out to evaluate different forms and modifications of MnO_2 as catalyst materials in composite electrodes for oxygen evolution. The focus was on studying the influences of catalyst fraction and catalyst particle size on the overall activity of the composite anode material.

The catalytic properties of MnO_2 to evolve oxygen have been well described in acidic media [84–90]. Common problems for this electrode material are the contact resistance between the current carrying support, usually titanium, and the catalytic layer, its high resistivity [85] and deactivation of the electrode surface in acidic environments [86].

Studies on the use of MnO_2 for oxygen evolution have mainly been carried out on electrodes prepared by spray pyrolysis and thermal decomposition, resulting in β-MnO_2 [86, 89]. As an alternative, electrochemically deposited MnO_2 (EMD) has been investigated [91–93], which usually results in γ-MnO_2.

The Outotec cold-spraying method [80] has the advantage that the catalyst can be prepared ex situ and can then be easily sprayed onto the anode surface. With the exception of the 'Merrlin anode' technology mentioned earlier [63–65], ex situ preparation of MnO_2 for use in EW anodes does not appear to be widely reported.

Aside from the cost effectiveness of cold spraying (the carrier gas can be compressed air), as there is no heating, the catalyst composition and microstructure do not change when applied to the electrode surface.

A tablet pressing method was selected to produce composite samples, analogous to those given by cold spraying, for screening the MnO_2 catalysts, without the need to involve all the details of the spray coating procedure. In addition, the research shows in which way the properties of the composite electrode can be best exploited.

1.1 Composite electrodes

For making a cost efficient electrode assembly, it is required that the electrode is very active over a long time whilst displaying low ohmic losses [94].

The catalyst needs to form only a small fraction of the total anode, whilst the matrix element, which is usually a metal, serves as a current support. The matrix does not need to be electrochemically active and the matrix material also enhances the mechanical stability of the coating. The catalyst lowers the required electrode potential and also the corrosion of the electrode. For the fabrication of composite electrodes, it is common to use plating methods to codeposit electrocatalysts onto a matrix material, where a solution containing the electrocatalyst in the form of a suspension or as a solution precursor [94] is used.

1.2 MnO_2 modifications and microstructure

Manganese dioxide is a material with several modifications, of which the best known are referred to as $\alpha-\delta$. The different modifications are sketched in Table 1.

α-MnO_2 consists of an octahedral network with a 2×2 tunnel structure. Pyrolusite or β-MnO_2 is seen as the most stable modification, consisting of octahedra that form a 1×1 tunnel structure by edge sharing. The abbreviation γ-MnO_2 stands for a two-phase mixture of pyrolusite and ramsdellite and δ-MnO_2 consists of a layered octahedral structure [95].
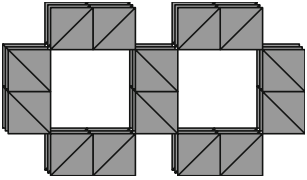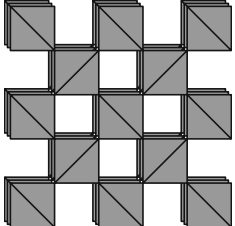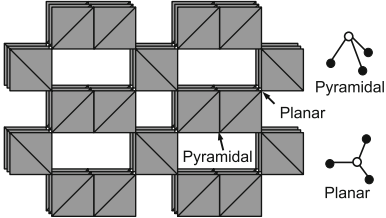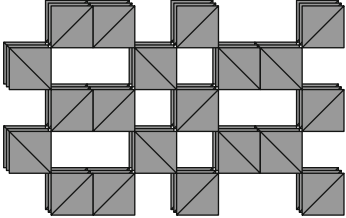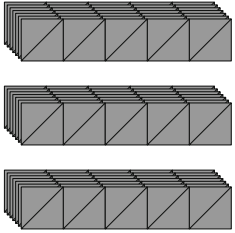
The ramsdellite structure is made up by a different edge sharing of octahedra, which form a 2×1 tunnel structure.

Whilst β-MnO_2 is usually low-defect, γ-MnO_2 contains additional point defects (Mn^{3+} and water content [96]), and so is also referred to as MnO_x, and can contain micro twinning defects [95].

These defects have been used, together with the composition of γ-MnO_2, to describe its conductivity and its semiconducting properties [96, 97]. An interdependence between the acid base properties and the composition of γ-MnO_2 has been suggested [96].

γ-MnO_2 is thus difficult to characterise [95]. Since the defects and the material properties are mostly dependent on the preparation method, it is often described as CMD for chemically prepared MnO_2, EMD for electrochemically prepared MnO_2, AMD for activated MnO_2 etc.

Table 1 Modifications of MnO$_2$, sketch after Chabre and Pannetier [95]

Phase name	Crystal structure's names/description	Sketch
α	2 × 2 channels	
β	Pyrolusite, 1 × 1 channel	
	Ramsdellite, 2 × 1 channels, channels contain two different types of oxygen: in planar and pyramidal configuration	Pyramidal / Planar / Pyramidal / Planar
γ	Mixture of pyrolusite and ramsdellite	
δ	Layered structure	

These four manganese dioxide types have been extensively investigated for their key properties in battery applications, for example, discharge capacities [96] and resistivity [96, 97]. Hydrogen peroxide decomposition [98] has also been studied. However, to our knowledge, the effectiveness of the different modifications as oxygen evolution electrocatalysts has not been reported.

2 Experiments

Five different MnO$_2$ samples were tested. Three were commercial: "M-2016" from Cerac Inc., USA (β-MnO$_2$), and "K60" (EMD) and "Faradiser M" (CMD1) both from Erachem Comilog Inc., USA. Two further CMD samples were prepared by synthesis.

2.1 MnO_2 synthesis

All chemicals used for the synthesis were of reactant grade or better and the water used was distilled.

2.1.1 Synthesis I: CMD2

In a 5-L flask, a solution of ca. 200 g L^{-1} HNO_3 containing 50 g L^{-1} $Mn(NO_3)_2$ was prepared by dissolving 100 g $Mn(NO_3)_2 \cdot xH_2O$ in a 2 L solution containing 1/3 conc. HNO_3 and 2/3 water. Magnetic stirring was used and 70 g of $NaClO_3$ powder were added to the flask; an immediate change in colour to brown/black was observed as MnO_2 started to precipitate.

The solution was stirred for approximately half an hour, and 2 L of distilled water was added and left another half hour stirring before setting the flask aside overnight. The following day, it was filtered with a fine filter paper (Schleicher & Schuell Micro Science 598/2), washed with 2 L of water and dried in a vacuum oven for 3 h at 60 °C and ca. 20 mbar (VTR 5022, Heraeus, Germany).

2.1.2 Synthesis II: CMD3

A 166 g L^{-1} H_2SO_4 solution with 50 g L^{-1} $MnSO_4$ solution was prepared in a 5-L flask by first dissolving 100 g $MnSO_4 \cdot H_2O$ in 400 mL water, adding 333 g H_2SO_4 and adding water to give a volume of 2 L. This mixture was heated to boiling on a magnetic stirrer/heater plate (VMS-C7, VWR, Germany). At ca. 40 °C, $NaClO_3$ (70 g) was added as powder to the flask. With the heating, the colour of the solution changed first from very pale pink to an increasingly red/brown colour and finally a black solution with precipitates. When the solution started boiling, the formation of Cl_2 gas was noted, but after a short time, it stopped.

The reaction was allowed to continue for 2.5 h at the maximum temperature setting of the heater plate, after which the heating was stopped and 2 L of distilled water

was added to the reactor. The stirring was continued for a further half hour, after which the solution was set aside overnight then filtered, washed and dried as per synthesis I.

2.2 Sample preparation

In order to classify the synthesised material, an XRD powder diffractometer (PW 1050/81, 1710/00, 3830/00, Phillips, Netherlands) was used.

The powder needed for the pressed composite electrodes was prepared by mixing lead powder (~200 mesh, 99.9% from Alfa Aesar, Karlsruhe, Germany) with a sample of the catalyst under investigation (usually 10 wt% MnO_2, unless otherwise stated). For the preparation of the electrode tablet, first, the base of the tablet was pressed with lead powder (11 tonne load for 20 s), the piston of the pressing tool was removed and 1 g of the mixed composite powder was added on top of the lead disc, and then the piston was replaced and pressed again (11 tonne load for 10 min). For the electrical contact, a lacquered copper wire (0.5 mm) was soldered to the back of the tablet and insulated with a non-conducting lacquer (E71524 lacquer, Markwins, Germany).

For electrolytic tests, the pressed tablet was inserted into an in-house manufactured Teflon electrode assembly (see Fig. 1b), ground with 1,200 grit paper and polished with 0.3 μm Al_2O_3 suspension (Micropolish II, Buehler, USA) using a polishing wheel (Motopol 8, Buehler, USA).

The second component of the assembly consisted of a Luggin capillary, into which the reference electrode (SSE, $Hg/Hg_2SO_4 = +0.615$ V vs. NHE) was inserted and a hole through which the Pt counter electrode was inserted. Both components were then attached together with stainless steel screws. The fixed positions of all three electrodes ensured reproducibility of the cell geometry.

The samples tested are listed in Table 2. For samples 14–17, the CMD1 powder was sieved into four size fractions, where successively smaller size grading sieves were used.

Fig. 1 **a** Electrode assembly made of PTFE, fixed positions of Luggin capillary and working electrode. **b** Pressed tablet electrode consisting of lead base and mixed Pb–MnO_2 composite
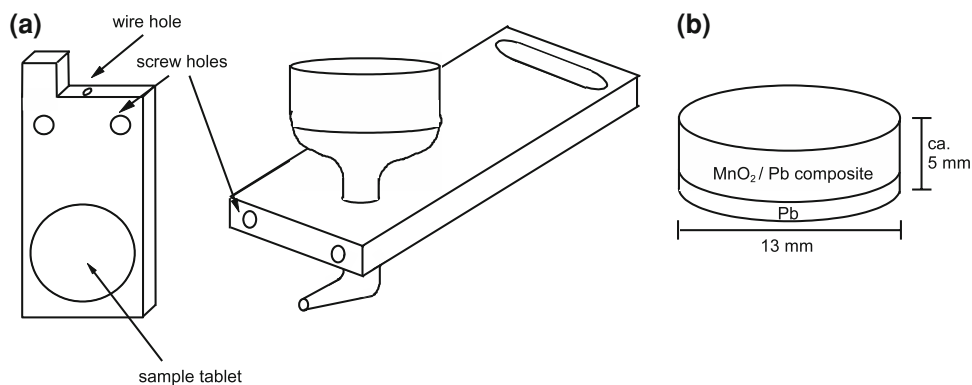
(a) wire hole
screw holes
sample tablet

(b) MnO_2/ Pb composite
Pb
ca. 5 mm
13 mm

Table 2 Pressed Pb/MnO$_2$ electrodes used during the tests

No.	Purpose	Type MnO$_2$	MnO$_2$ (wt%)
1–3	Different MnO$_2$ modifications	Pyrolusite/EMD/CMD	5
4–6	Different MnO$_2$ modifications	CMD1/CMD2/CMD3	10
7–13	Role of the surface percentage	CMD1	3, 5, 10, 15, 20, 25, 30
14–17	Role of the MnO$_2$ particle size	20–25, 25–32, 32–37, 37–45 μm CMD1	10

2.3 Sample testing

The electrochemical testing was conducted in a thermostated flow cell with a volume of ca. 150 mL placed inside a Faraday cage. All other electrical equipment was placed outside of the Faraday cage. The electrolyte solution was 160 g L^{-1} H$_2$SO$_4$, prepared from analytical grade H$_2$SO$_4$, and Milli-Q grade water (Millipore, USA) was thermostated to 37 °C (thermostat DC3, Haake, Germany) and flowed through the cell with a peristaltic pump (IPS 12, Ismatec, Switzerland) at a rate of 1 mL/min.

The testing procedure was executed by a macro program in the GPES software controlling the Autolab PGStat 100 potentiostat (EcoChemie, Netherlands), which ensured that the testing procedure for every sample was identical.

The macro program contained the following steps:

Step 1: Preconditioning of the electrode was carried out galvanostatically with a current density of 57 mA cm^{-2} for 1 h.
Step 2: Equilibration was done at the open circuit potential for 5 min to avoid cathodic currents in the following sweep
Step 3: Three cyclic voltammetry (CV) sweeps were made from 0.9 to 1.6 V vs. SSE (or to 280 mA, the limit of the potentiostat) at a sweep rate of 0.5 mV s^{-1}.
Step 4: The following galvanostatic electrochemical impedance program was run for the currents 1, 20, 40, 60, 80 and 100 mA (with amplitudes 0.5, 2, 4, 6, 8 and 10 mA, respectively):

- 30-min equilibration at the given current whilst measuring the ohmic resistance (1,150 Hz, at an interval of approximately 3 s).
- A frequency scan from 10 Hz to 10 kHz with 100 data points.

The *iR* drop corrections were carried out using the mean value of the ohmic resistance gained in the equilibration of step 4 at 80 mA. For comparison purposes, a tankhouse lead anode material, alloyed with 0.6% silver (PbAg0.6) was measured.

3 Results

All potential values are represented as *iR* corrected and refer to the SSE reference electrode

3.1 XRD results

The results from the XRD measurements can be seen in Fig. 2. The CMD3 sample can be described as highly crystalline α-MnO$_2$ with all typical peaks present for that material [99].

XRD measurements of the CMD2 MnO$_2$ sample, produced by the low temperature method (synthesis I), showed that it had poor crystallinity (amorphous or very small crystals); however, the main peaks can still be seen. Since one important peak of the γ-MnO$_2$ modification can be seen (22°) and two peaks (at ca. 18° and 28°) typical of the alpha modification are missing, this was classified as γ-MnO$_2$ [95, 99].

3.2 Effect of the modification on O$_2$ evolution reaction

The modification of MnO$_2$ is important; both the chronopotentiometric response measured during the preconditioning stage described in step 1 of Sect. 2.3 (shown in
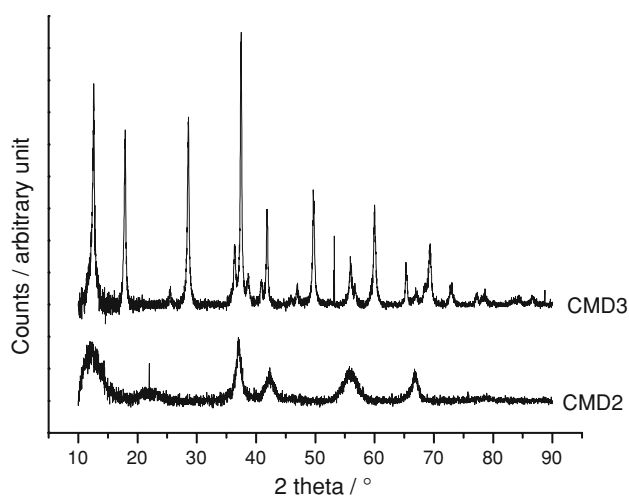
Fig. 2 XRD results from synthesised powders CMD2 identified as γ-MnO$_2$ and CMD3 as α-MnO$_2$

Fig. 3) and the polarization curves shown in Fig. 4 support this idea. The PbAg0.6 anode material from the zinc tankhouse was clearly the least active of those tested. β-MnO_2 was observed to be 0.25 V more active, whilst EMD was a further 0.05 V more active. CMD1 was 0.35 V more active than PbAg0.6 in solutions containing no manganese and was clearly the best catalyst.

In addition, there were differences in activity between the three CMD samples tested (Fig. 5); the synthesised CMD2 (γ-MnO_2) was found to be most active while the commercial CMD1 and CMD3 (α-MnO_2) had similar electrochemical activities.

Fig. 5 Potential sweep for 10 wt% pressed samples, ■ = commercial CMD1, ● = synthesised CMD2, ▲ = synthesised CMD3
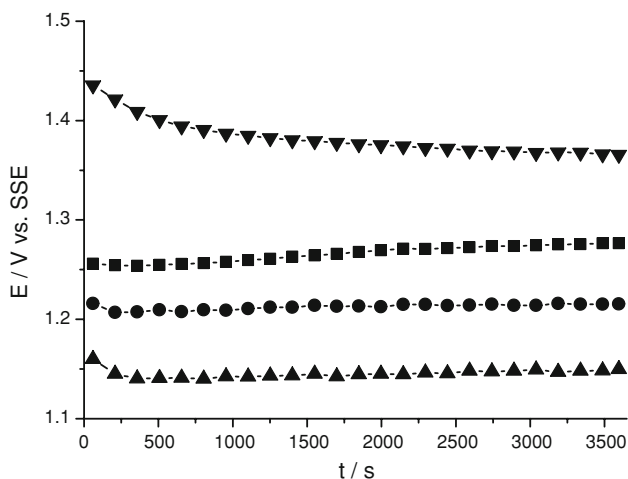

Fig. 3 Galvanostatic response during the preconditioning stage for three commercial MnO_2 samples (using 5 wt%), also a tankhouse PbAg lead anode material. $[H_2SO_4] = 160$ g L^{-1}, $T = 37$ °C, ■ = β-MnO_2, ● = EMD and ▲ = CMD1 and ▼ = PbAg
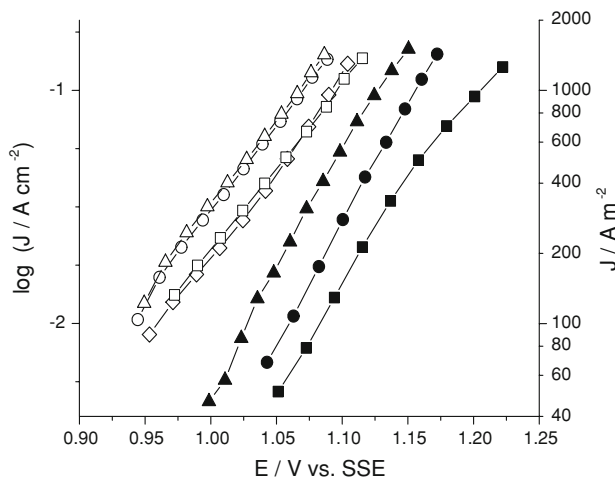
Fig. 6 Potential sweep for tablet electrodes with different wt% of CMD1: ■ = 3%, ● = 5%, ▲ = 10%, ◇ = 15%, □ = 20%, ○ = 25%, △ = 30%

3.3 Effect of the composite electrode properties

The influence of the fraction of MnO_2 in the pressed tablet on the geometrical current density is seen in Fig. 6. With an increase from 3 to 15 wt% MnO_2, the voltage required to pass a given current density decreases, but when going above 15 wt% MnO_2, the trend in the decrease in potential is no longer clear. This can be explained by poor mechanical stability when using larger weight fractions of the MnO_2 powder.

Current density was observed to increase with decreasing particle size and was found to be inversely proportional to the average MnO_2 particle radius (r) as seen in Fig. 7. The particle size experiments were carried out in duplicate, and the results were found to be reproducible.
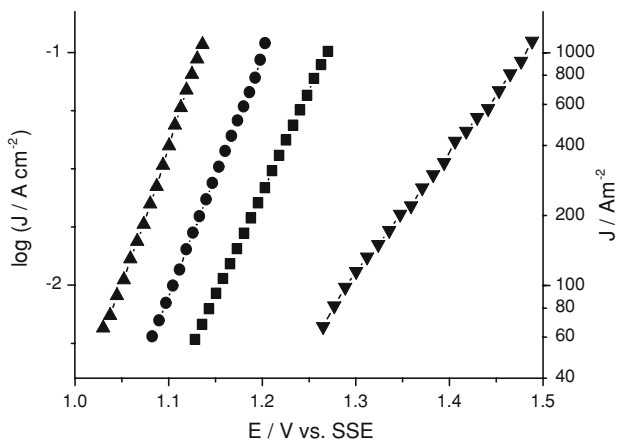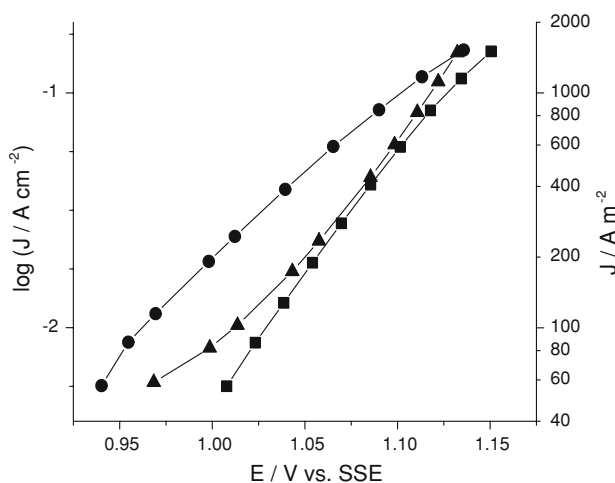

Fig. 4 Polarisation curves for three commercial manganese dioxides (using 5 wt%), also a tankhouse PbAg lead anode material. $[H_2SO_4] = 160$ g L^{-1}, $T = 37$ °C, ■ = β-MnO_2, ● = EMD and ▲ = CMD1 and ▼ = PbAg
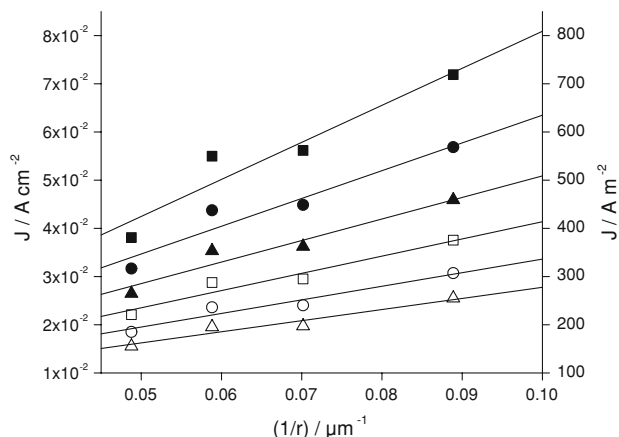
Fig. 7 The effect of the mean CMD particle size (22.5, 28.5, 34 and 41 μm diameter) on the current density (CMD electrode). The symbols refer to *iR* corrected applied potentials vs. SSE reference electrode (■ = 1.10 V, ● = 1.09 V, ▲ = 1.08 V, □ = 1.07 V, ○ = 1.06 V, △ = 1.05 V)

3.4 A general model for active boundaries

It can be shown that a $1/r$ catalyst particle size dependence is obtained when assuming that the main active area of a particle is around its circumference.

In such a model, the current (i) through the electrode is then proportional to the sum of the boundary lengths (Σl) of all catalyst particles.

A cross section of a random distribution of spheres in a cube volume can be approximated as being the same as the cutting of a single sphere n times. Since the cutting ($r_{cut} = \sqrt{r^2 - h_{cut}^2}$, Fig. 8) is equally distributed in cutting height h_{cut}, the result is that cutting the sphere at the
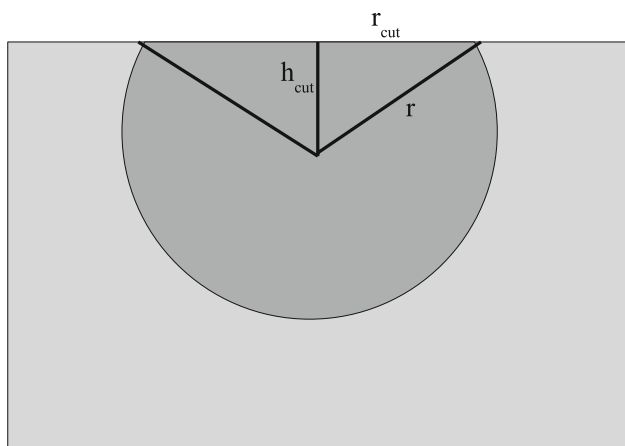

Fig. 8 Schematic of a cut catalyst particle resulting from polishing of the composite electrode samples

highest possible radius has the highest probability, whilst cutting it at small radii is less probable.

The mean cutting radius can be described in the following way:

$$\bar{r}_{cut} = \frac{1}{2r} \int_{-r}^{r} \sqrt{r^2 - h^2} \, dh = \frac{\pi}{4} r \qquad (2)$$

Therefore, the mean cutting radius $\bar{r}_{cut}$, is directly proportional to the particle radius r. The number of particles at the electrode surface, N_p, is given by (3):

$$N_p = A_{Geom} \Theta / \bar{A}_p \qquad (3)$$

where Θ is the catalyst surface coverage, A_{Geom} is the geometric surface area and $\bar{A}_p$ is the average area of one particle.

The total boundary length (Σl) is a product of N_p and $2\pi \bar{r}_{cut}$, and the average particle area is a function of the particle radius squared:

$$\bar{A}_p = \pi \frac{1}{2r} \int_{-r}^{r} r^2 - h^2 \, dh \qquad (4a)$$

$$\bar{A}_p = \frac{2}{3} \pi r^2 \qquad (4b)$$

The total length Σl of the particle boundaries is then inversely proportional to the catalyst particle radius, r (5b).

$$\Sigma l = N 2\pi \bar{r}_{cut} = \frac{A_{Geom} \Theta}{2/3\pi r^2} \frac{2\pi^2 r}{4} \qquad (5a)$$

$$\Sigma l = \frac{3\pi}{4} \frac{A_{Geom} \Theta}{r} \qquad (5b)$$

Assuming that the surface coverage Θ is equivalent to the volume fraction (vol%), then the total current i can be expressed as follows:

$$i = nFBK\Sigma l \qquad (6a)$$

$$i = 3/4\pi nFBK \frac{A_{geom} \, vol\%}{r} \qquad (6b)$$

where k is a potential-dependent electrochemical rate constant, n is the number of transferred electrons, F is the Faraday constant and B is a proportionality factor which accounts for the electrochemically active species involved in the reaction kinetic expressions.

This model could also be extended to non-spherical particles, with non-circular cross sections; however, in the present studfy, it is assumed that the MnO$_2$ particles are approximately spherical.

If the boundaries between the matrix and the catalyst particles are indeed the most active part of the composite electrode surface under oxygen evolving conditions, then the current will be inversely proportional to the

characteristic dimensions. In such cases, the particles with the smallest characteristic dimensions will be most active, as they have the highest ratio of circumference to surface area.

4 Discussion

4.1 Influences of the different modifications of MnO$_2$

Figures 3, 4 and 5 show that for a current density of 60 mA cm^{-2} (600 A m^{-2}), a composite electrode containing CMD2–MnO$_2$ catalyst showed an oxygen evolution electrode potential of ca. 1.1 V against the SSE, which was 0.25–0.30 V lower than for a standard PbAg0.6 electrode. For comparison, PbAg0.6 in manganese containing solutions is reported to give a voltage of ca. 1.35 V against the SSE [31], meaning that the CMD2 lead composite tested in the present study is ca. 0.25 V more active than the usual case.

The chemical and electrochemical activity of MnO$_2$ depends strongly on the modification. Ramsdellite blocks contain oxygen atoms in both pyramidal and planar positions [95], β-MnO$_2$ lacks ramsdellite blocks, whilst in CMD, there are typically higher concentrations than in EMD [99] α-MnO$_2$ such as CMD3 should contain even more oxygens in pyramidal positions, and so was expected to be more active for oxygen evolution; however, CMD3 was not as active as predicted.

For composite electrodes, the contact resistance between the catalyst and the matrix metal is especially important. It is known from Zn electrowinning that the γ-MnO$_2$ (EMD), which grows on the anode surface during electrolysis, does not adhere well to a lead (or lead oxide) anode surface. Also, the intrinsic conductivity of the catalyst will play a role, depending on the water content and defect structure [96], which is different for α-MnO$_2$, β-MnO$_2$, EMD and CMD [95, 99]. EMD is defect rich, whilst CMD has less defects [95].

4.2 Characteristics of the results compared to the presented model

The experimental data showed an inversely proportional relationship between current density and particle radius and therefore catalyst volume or surface percentage.

It should be noted that the present model approximates that the current flows exclusively through the boundary between the catalyst particles and the lead matrix. A more realistic description would be that a region of certain width would be the most active area covering the edge of the MnO$_2$ (ring shape); however, the present approximation is sufficient as we are only looking for physical and electrochemical processes that might induce such behaviour.

4.3 Influences of physical and electrochemical mechanisms and composite electrode properties

The physicochemical properties of composite electrodes, such as those formed when MnO$_2$ is cold spray coated or pressed onto a lead support, are complex. Size and fraction of MnO$_2$ catalyst have a strong influence on the electrode activity. In order to identify the mechanisms at work, these are presented and their impact on the anode activity is assessed.

4.3.1 Bulk volume properties

The MnO$_2$ catalysts used are brittle ceramic materials with high resistivities, meaning that during the fabrication of composites, the catalyst particles must not be crushed. Assuming spherical catalyst particles, then a dense packed structure will have a maximum percentage of 74.05 vol% [100]. The mechanically stable limit, however, is ca. 30 wt% (ca. 50 vol%) of MnO$_2$ catalyst, after which the pressed samples become too fragile to be useful for testing. The other important function of the Pb matrix is to provide the bulk conductivity of the electrode, as shown in Fig. 9. This means that the conducting matrix part of the electrode must provide a path for the current to flow through the bulk of the material.

The contribution of the electrode's resistivity to the total iR drop can be evaluated by comparing electrodes with different catalyst fractions. The iR drop caused by the solution resistance can be considered to be constant when the positions of the electrodes are fixed. The total ohmic drop was relatively small in all cases (several mV, at most 10 mV) and all results presented here were iR corrected. An increase in total ohmic resistance could be seen for higher catalyst fractions.

4.3.2 Inner catalyst particle resistance

At the surface of the composite electrode, where the current must pass into the catalyst, the internal resistance of the catalyst particle is important (marked as c in Fig. 9).

The conductivity of MnO$_2$ is several orders of magnitude lower than that of metals [96, 97]. When the particle size increases, a higher potential drop can occur due to the higher resistance path, which electrons must take through the MnO$_2$ particle. It is logical that the current distribution will be such that the current density is highest at the particle/matrix boundary but there will be lower current density towards the centre. If the current is decreasing steeply from the boundary, then the premises of the presented

Fig. 9 Sketch to demonstrate bulk properties and electric properties of composite electrodes: (a) Catalyst particles are well embedded into the electrode: mechanically stable; good conductivity. (b) Too low amount of matrix to interconnect; mechanical instability and high resistivity. (c) The highest current density is expected at the edge of the catalyst particle
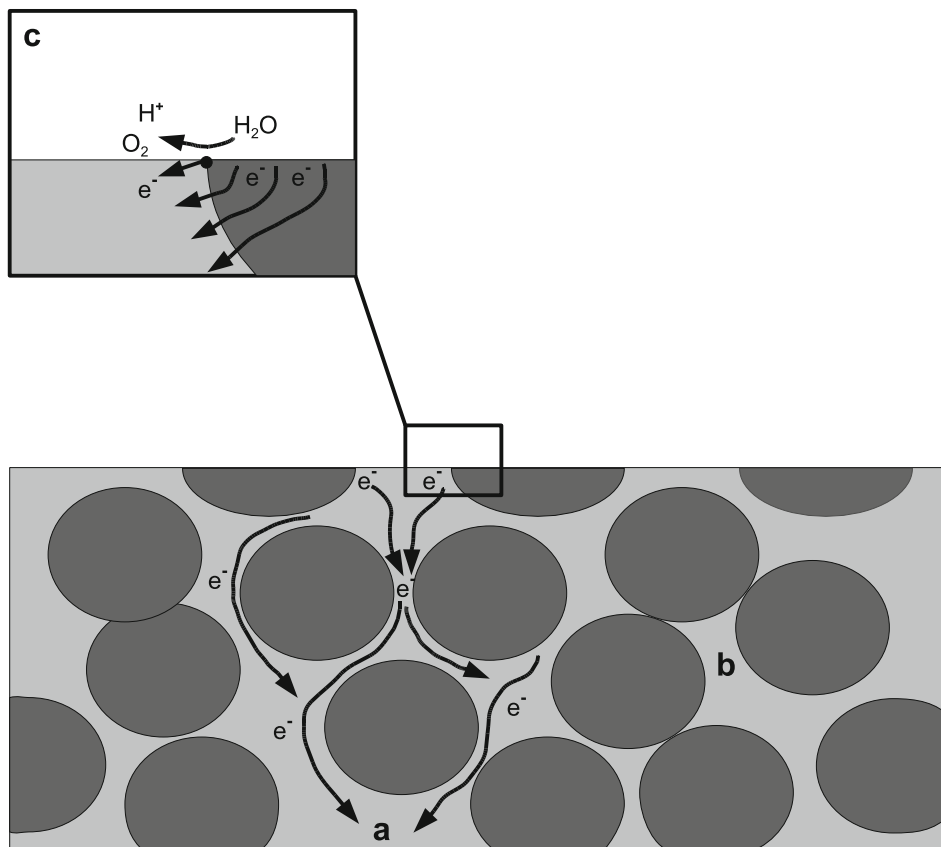
model are fulfilled, which leads to an inversely proportional relationship between particle radius and current density at the composite electrode.

4.3.3 Mass transport of sulphuric acid and oxygen

For large, homogenous electrodes, the electrochemical edge effects at the boundary between active and inactive areas can be neglected. For microelectrodes, however, where $r < 50$ μm, mass transport rates are high due to spherical diffusion [101].

Since the MnO_2 catalyst particles used in the present study have sub 50 μm diameters, the composite electrode surface can be considered as an array of microelectrodes [102–105], where the neighboring particles are close to each other, and at steady state, the diffusional fields overlap, as shown in Fig. 10.

Since the solvent is water, there is no reason to consider its mass transport. Mass transport of oxygen and protons could affect the performance of the composite electrode, because they are involved in the kinetics and thermodynamics of the water oxidation reaction (1).

Fig. 10 Sketch of the diffusion fields of protons and molecular dissolved oxygen that are overlapping
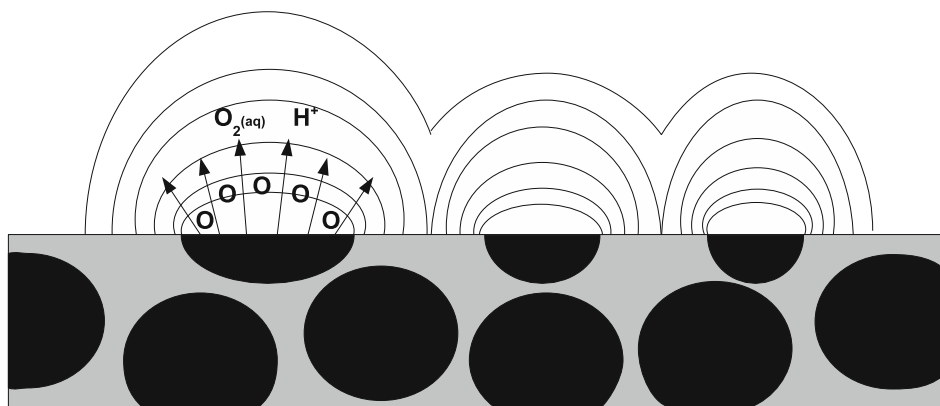
The concentration build up of oxygen can be considered to be high, compared to its bulk concentration at saturation, ca. 0.5 mmol L^{-1} [106, 107]. Most of the oxygen evolved is lost as gas bubbles formed on the electrode, the formation of which requires a supersaturation of dissolved oxygen, which has been measured by Janssen and Barendrecht [108, 109].

For protons, it should be considered that the electrolyte does not contain any supporting salt and thus the movement of protons is coupled to the movement of [HSO$_4$]$^-$ due to electroneutrality. The process is then diffusion of sulfuric acid, which is a much slower process than separate movement of protons ($D_{H_2SO_4}^{\pm} \approx 2.2 \times 10^{-5}$ cm^2 s^{-1} [110]).

Due to the high degree of overlap between the diffusional fields of the individual catalyst spots, this could normally be accessed as a linear diffusion problem. However, since we are interested in the current distribution at an average catalyst particle spot, we also have to consider that proton and oxygen concentrations will be lower at the boundaries (inverse edge effects), permitting a higher current flow at the edges around the boundary of the particle.

Whether the spherical diffusion improves the mass transport of oxygen or sulfuric acid significantly or not cannot be easily answered.

4.3.4 Gas evolution

Gas evolution phenomena are the most complicated processes involved in the overall system. Surface energy or surface tension is a key aspect for all properties of bubbles: It determines the spots where bubbles will nucleate, on which area they will reside (generally on the more hydrophobic area), how easily a bubble will start to move and detach from the electrode and how large those bubbles will be [73, 111–113]. The composite electrode used here is different from a plain Pb electrode, which is usually much more homogenous and does not have areas of alternating properties as given by spray-coating or pressing with MnO$_2$.

When a gas bubble sits on the surface, the equilibrium between the surface tensions (γ) can be described by the contact angle between the gas bubble and the electrode. This results in an 'inverse' Young's equation (7) [112], which is similar to the drop on a solid problem. Consequently, the gas solid contact angle (θ_{GS}) and the liquid solid contact angle (θ_{LS}) add up to 180° (8).

$$\cos \theta_{GS} = \frac{\gamma_{SL} - \gamma_{GS}}{\gamma_{GL}} = -\cos \theta_{LS} \tag{7}$$
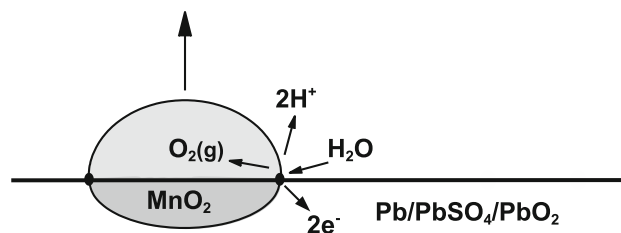
$$\theta_{GS} = \pi - \theta_{LS} \tag{8}$$

Fig. 11 Sketch of bubble growth on the catalyst. The boundary is still free of electrochemical reactions

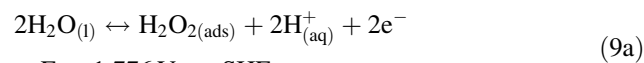where the subscripts G, L and S indicate gas, liquid and solid, respectively.

Bubbles can nucleate and grow on the hydrophobic area of the electrode more easily than on the hydrophilic areas, which are better wetted by electrolyte solution and might even detach from the surface before spreading out onto the hydrophilic area.

The boundaries would then be free for electrochemical reactions (see Fig. 11) for the maximum amount of time. In a certain time span of the bubble growth, the assumptions of the presented model are met because everywhere but the boundary of the catalyst would be blocked.
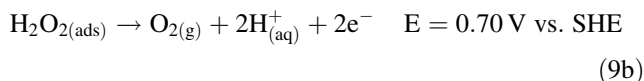
4.3.5 Special electrochemical reactions at the catalyst matrix boundary

Two-step mechanisms with short living intermediates (Fig. 12, step 1 on the matrix step 2 on the catalyst) could also produce the same 1/r relationship with current. As a hypothetical example, hydrogen peroxide is assumed to be produced as an intermediate:

Reaction (9a) would take place on the lead matrix, which determines the potential of the electrode. A further oxidation reaction (9b) would occur on the MnO$_2$ under limiting current conditions (as the voltage required for this reaction is much lower):

$$2H_2O_{(l)} \leftrightarrow H_2O_{2(ads)} + 2H_{(aq)}^+ + 2e^-$$
$$E = 1.776 \text{ V vs. SHE} \tag{9a}$$

$$H_2O_{2(ads)} \rightarrow O_{2(g)} + 2H_{(aq)}^+ + 2e^- \quad E = 0.70 \text{ V vs. SHE} \tag{9b}$$

Since the second step of the oxidation reaction (9b) occurs at limiting current density, the region of the catalyst
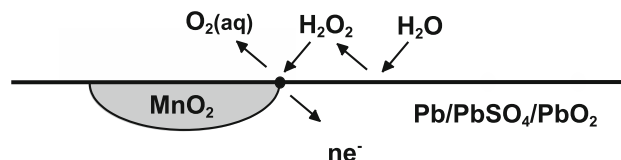

Fig. 12 Two-step reaction, where step 1 proceeds on the matrix and step 2 on the catalyst

particle closest to the metal matrix will consume most of the H_2O_2. This results in a high local current density at the MnO_2 particle/Pb matrix boundary.

4.3.6 Total impact of all mechanisms

The presented mechanisms support the proposal that the MnO_2 particle boundaries have particular properties, which make them more active than the rest of the catalyst surface.

For all of the presented mechanisms, we have shown that the assumptions of the model are met. The effect of the MnO_2 catalyst particle radius is distinct, even for relatively small changes in MnO_2 particle radius from 10 to 20 μm, and the effect increases with increasing electrode potential.

In particular, both conductivity at the composite electrode surface and mass transport are dependent on the current density used, which will be reported elsewhere.

5 Conclusion

The influence of different modifications on the ability of MnO_2 to catalyse the oxygen evolution reaction in strongly acidic media was investigated. Ex situ methods were used to synthesise the MnO_2 catalysts particles and produce composite tablet electrodes with up to 30 wt% of MnO_2. Both α and γ CMD were found to be more active than EMD and β-MnO_2, whilst γ-CMD was approximately 0.25 V more active than the standard lead silver alloy anode used in Zn EW.

These results indicate that an inexpensive electrocatalyst (MnO_2) and economic coating method (cold spraying) could lead to a considerable improvement in the oxygen evolution overpotential for Zn electrowinning, equating to an approximate 5% saving of electrical energy used. The main benefit is that this coating system could be introduced as an extension of the traditional lead anode technology.

Several possible physical and electrochemical reasons have been given that explain the experimental results. The main reason being because of the much higher performance of small fractions of catalyst compared to the standard lead–silver alloyed electrodes (where the whole surface is covered with MnO_2) makes it reasonable to suggest that composite electrodes have a significant advantage.

Further investigations will focus on elucidating the local processes on the microscopic scale, starting with investigating mass transfer effects using scanning electrochemical microscopy (SECM) and rotating disc electrode (RDE). Another urgent aspect that needs to be clarified is the long-term stability and performance of these particular composite electrodes; to date, the longest time a pressed tablet sample was tested was 6 h (the duration of one experiment). MnO_2 cold spray coated PbAg anodes have shown good performance in initial industrial Zn EW tests, which will be reported elsewhere.

References

1. Rerolle C, Wiart R (1996) Electrochim Acta 41:1063
2. Aromaa J, Evans JW (2007) Encycl Electrochem 5:159
3. Felder A, Prengaman RD (2006) JOM 58:28
4. Amadelli R, Maldotti A, Molinari A et al (2002) J Electroanal Chem 534:1
5. Yu P, O'Keefe TJ (1999) J Electrochem Soc 146:1361
6. Pavlov D, Monahov B (1996) J Electrochem Soc 143:3616
7. Cachet C, Rerolle C, Wiart R (1996) Electrochim Acta 41:83
8. Hyvärinen O (1972) Doctoral thesis: the effect of silver and cobalt on the oxygen evolution at lead anodes. Helsinki University of Technology, Espoo
9. Yu P, O'Keefe TJ (2001) Proceedings of the 31st annual hydrometallurgy meeting. Toronto, p 129
10. Schulze-Messing J, Alexander DC, Sole KC et al (2007) Hydrometallurgy 86:37
11. Zhang W, Cheng CY (2007) Hydrometallurgy 89:178
12. Niemi M (2007) Master's thesis: the influence of process parameters on zinc electrolysis. Helsinki University of Technology, Espoo
13. Gnoinski J, Bachmann T, Holtzhausen S (2005) Conference proceedings lead & zinc '05. Kyoto, p 1315
14. Yu P, O'Keefe TJ (2002) J Electrochem Soc 149:A558
15. Pajunen L, Aromaa J, Forsén O (2003) Proceedings of the 5th international symposium of hydrometallurgy, vol 2. Vancouver, p 1255
16. Ivanov I, Stefanov Y, Noncheva Z et al (2000) Hydrometallurgy 57:109
17. Bombach H, Stelter M, Mohr KP et al (2003) Metall 57:386
18. Stelter M, Bombach H, Saltykov P (2005) BHM 150:1
19. Siegmund A, Prengaman D (2003) Proceedings of the 5th international symposium of hydrometallurgy, vol 2. Vancouver, p 1279
20. Hein K, Duman I, Timur S (1994) Metall 48:532
21. Timur S, Hein K (1995) Metall 49:496
22. Stelter M, Hein K, Bauer I (1998) Proceedings of an international symposium on zinc and lead processing. Calgary, p 389
23. Rodrigues JMS, Meyer EHO (1996) EPD congress, proceedings of sessions and symposia held at the TMS annual meeting. Anaheim, p 161
24. Gonzalez JA (2001) Proceedings of the 31st annual hydrometallurgy meeting. Toronto, p 147
25. Ivanov I, Stefanov Y, Noncheva Z et al (2000) Hydrometallurgy 57:125
26. Hrussanova A, Mirkova L, Dobrev T (2001) Hydrometallurgy 60:199
27. Hrussanova A, Mirkova L, Dobrev T (2002) J Appl Electrochem 32:505
28. Hrussanova A, Mirkova L, Dobrev T et al (2004) Hydrometallurgy 72:205
29. Hrussanova A, Mirkova L, Dobrev T (2004) Hydrometallurgy 72:215
30. Stelter M, Hein K, Bauer I (1998) Erzmetall 51:281

31. Rashkov S, Dobrev T, Noncheva Z et al (1999) Hydrometal-lurgy 52:223
32. Moats MS (2008) JOM 60:46
33. Beer HB (1961) Ger. Pat. Appl. 1115721
34. Beer HB (1966) Neth. Pat. Appl. 6606302
35. Beer HB (1972) US Patent 6800834
36. Beer HB (1976) US Patent Reissue 28820
37. Beer HB, Hinden JM (1981) Eur. Pat. Appl. 27051
38. Beer HB, Hinden JM (1982) Eur. Pat. Appl. 46447
39. Hinden JM, Beer HB (1982) Eur. Pat. Appl. 46449
40. Chandler GK, Genders JD, Pletcher D (1997) Platin Met Rev 41:54
41. Hayfield PCS (1998) Platin Met Rev 42:27
42. Hayfield PCS (1998) Platin Met Rev 42:46
43. Pavlovic MG, Dekanski A (1997) J Solid State Electrochem 1:208
44. Cobley AJ, Gabe DR, Graves JE (2001) Trans Inst Met Finish 79:112
45. Chen G (2004) Sep Purif Technol 38:11
46. Cardarelli F, Taxil P, Savall A et al (1998) J Appl Electrochem 28:245
47. Hayfield PCS (1998) Platin Met Rev 42:116
48. Robinson D, MacDonald S, Todaro F (2003) Proceedings—electrochemical society—electrochemistry in mineral and metal processing VI, vol 18, Paris, France, p 355
49. Wang S (2008) JOM 60:41
50. Treasure PA (2003) Proceedings—electrochemical society—electrochemistry in mineral and metal processing VI, vol 18, Paris, France, p 367
51. Bestetti M, Ducati U, Kelsall GH et al (2001) Can Metall Quart 40:451
52. Thonstad J (1998) Elektrolyseprosesser. Norwegian University of Science and Technology, Trondheim
53. Åkre T (2008) Doctoral thesis: electrowinning of cobalt from chloride solutions—anodic deposition of cobalt oxide on DSA. Norwegian University of Science and Technology, Trondheim
54. Nijjer S (2000) Doctoral thesis: deposition and reduction of manganese dioxide on alternative anode materials in zinc electrowinning. Norwegian University of Science and Technology, Trondheim
55. Da Silva LM, Boodts JFC, De Faria LA (2001) Electrochim Acta 46:1369
56. Chen X, Chen G (2005) J Electrochem Soc 152:J59
57. Shrivastava P, Moats MS (2008) J Electrochem Soc 155:E101
58. Beer HB (1982) Eur. Pat. Appl. 46727
59. Beer HB, Katz M, Hinden J (1983) Eur. Pat. Appl. 87186
60. Ferdman A (2000) US Patent 6129822
61. Chmiola J, Gogotsi Y, Ferdman A (2003) Sci Sinter 35:75
62. Weems D, Schledorn M, Farmer MD (2005) An insoluble titanium-lead anode for sulfate electrolytes. Available via DIALOG: http://www.osti.gov/bridge/servlets/purl/840009-oPsbtt/840009.PDF. Accessed 24 Oct 2008
63. Dattilo M (1997) US Patent 5632872
64. Dattilo M, Lutz LJ (2001) Proceedings of the 31st annual hydrometallurgy meeting. Toronto, p 447
65. Dattilo M, Lutz LJ (1999) Proceedings of the 4th COPPER-COBRE international conference, vol 3. Phoenix, p 597
66. Hardee KL, Moats MS (2000) Proceedings—electrochemical society—electrochemistry in mineral and metal processing V, vol 14, Toronto, Canada, p 294
67. Moats M, Hardee K, Brown C Jr (2003) JOM 55:46
68. Alfantazi AM, Moskalyk RR (2003) JOM 55:49
69. Wiesener K, Schneider W, Moebius A (1989) J Electrochem Soc 136:3770
70. Bestetti M, Ducati U, Kelsall G et al (2001) Can Metall Quart 40:459

71. Csicsovszki G, Kekesi T, Toeroek TI (2005) Hydrometallurgy 77:19
72. Ho CN, Hwang BJ (1994) J Electroanal Chem 377:177
73. Tikka P (2006) Master's thesis: gas evolving lead anodes—Kaasun kehitys Lyijianodeilla (in Finnish language). Helsinki University of Technology, Espoo
74. Musiani M, Guerriero P (1998) Electrochim Acta 44:1499
75. Palmas S, Polcaro AM, Ferrara F et al (2008) J Appl Electrochem 38:907
76. Vertova A, Borgese L, Cappelletti G et al (2008) J Appl Electrochem 38:973
77. Brungs A, Haddadi-Asl V, Skyllas-Kazacos M (1996) J Appl Electrochem 26:1117
78. Veräjänkorva S (2005) Master's thesis: thermal spraying of catalytic materials. Tampere University of Technology, Tampere
79. Gaertner F, Stoltenhoff T, Schmidt T et al (2006) J Therm Spray Technol 15:223
80. Barker MH, Hyvärinen O, Osara K (2007) PCT Int. Appl. 2007045716
81. Cole PM, Sole KC (2002) J S Afr Inst Min Metall 8:451
82. Sole KC, Feather AM, Cole PM (2005) Hydrometallurgy 78:52
83. Olenius E (2002) Master's thesis: oxygen evolving catalytic oxide layers preparation and characterisation—Hapen kehitystä katalysoivien oksidikerrosten valmistus ja karakterisointi (in Finnish language). Oulu University, Oulu
84. Kokhanov GN, Agapova RA, Milova NG (1972) Elektrokhimiya 8:862
85. Kalinovskii EA, Shustov VA, Chaikovskaya VM et al (1976) Elektrokhimiya 12:1573
86. Morita M, Iwakura C, Tamura H (1977) Electrochim Acta 22:325
87. Gorbachev AK, Krech EE, Shmorgun VI (1977) Elektrokhimiya 13:1046
88. Morita M, Iwakura C, Tamura H (1978) Electrochim Acta 23:331
89. Morita M, Iwakura C, Tamura H (1979) Electrochim Acta 24:357
90. Yang J, Shu Y, Jiang H (1987) Zhongnan Kuangye Xueyuan Xuebao 18:98
91. Habazaki H, Matsui T, Kawashima A et al (2001) Scr Mater 44:1659
92. Matsui T, Habazaki H, Kawashima A et al (2002) J Appl Electrochem 32:993
93. El-Moneim AA, Kumagai N, Asami K et al (2005) Mater Trans JIM 46:309
94. Cattarin S, Musiani M (2006) Electrochim Acta 52:1339
95. Chabre Y, Pannetier J (1995) Prog Solid State Chem 23:1
96. Ruetschi P (1984) J Electrochem Soc 131:2737
97. Xia X, Li H, Chen ZH (1989) J Electrochem Soc 136:266
98. Kanungo SB, Parida KM, Sant BR (1981) Electrochim Acta 26:1157
99. Hill LI, Verbaere A, Guyomard D (2003) J Electrochem Soc 150:D135
100. Sloane NJA (1998) Nature (London) 395:435
101. Faulkner LR, Bard AJ (2001) Electrochemical methods, fundamentals and application, 2nd edn. Wiley, New York
102. Stulik K, Amatore C, Holub K et al (2000) Pure Appl Chem 72:1483
103. Davies TJ, Banks CE, Compton RG (2005) J Solid State Electrochem 9:797
104. Davies TJ, Compton RG (2005) J Electroanal Chem 585:63
105. Ordeig O, del Campo J, Munoz FX et al (2007) Electroanalysis 19:1973
106. Atkins PW (1998) Physical chemistry, 6th edn. Oxford University Press, Oxford

107. Kaskiala T, Salminen J (2003) Ind End Chem Res 42:1827
108. Janssen LJJ (1992) J Appl Electrochem 22:1091
109. Janssen LJJ, Barendrecht E (1984) Electrochim Acta 29:1207
110. Lobo VMM (1989) Handbook of electrolyte solutions. Elsevier, New York
111. Vogt H (1983) In: Yeager E, Bockris JOM, Conway BE, Sarangapani S (eds) Comprehensive treatise of electrochemistry, vol 6: electrodics, transport. Plenum Press, New York
112. Baum T, Satherley J, Schiffrin DJ (1998) Langmuir 14:2925
113. Lantelme F, Groult H (2004) J Electrochem Soc 151:D121